

Closed-Loop Robotic Manipulation of Transparent Substrates for Self-Driving Laboratories using Deep Learning Micro-Error Correction

Kelsey Fontenot
MIT
kelfon@mit.edu

Anjali Gorti
MIT
argorti@mit.edu

Iva Goel
MIT
ivagoel@mit.edu

Tonio Buonassisi
MIT
buonassisi@mit.edu

Alexander E. Siemenn
MIT
asiemenn@mit.edu

Abstract

Self-driving laboratories (SDLs) have accelerated the throughput and automation capabilities for discovering and improving chemistries and materials. Although these SDLs have automated many of the steps required to conduct chemical and materials experiments, a commonly overlooked step in the automation pipeline is the handling and reloading of substrates used to transfer or deposit materials onto for downstream characterization. Here, we develop a closed-loop method of Automated Substrate Handling and Exchange (ASHE) using robotics, dual-actuated dispensers, and deep learning-driven computer vision to detect and correct errors in the manipulation of fragile and transparent substrates for SDLs. Using ASHE, we demonstrate a 98.5% first-time placement accuracy across 130 independent trials of reloading transparent glass substrates into an SDL, where only two substrate misplacements occurred and were successfully detected as errors and automatically corrected. Through the development of more accurate and reliable methods for handling various types of substrates, we move toward an improvement in the automation capabilities of self-driving laboratories, furthering the acceleration of novel chemical and materials discoveries.

1 Introduction

In recent years, laboratory automation and self-driving laboratories (SDLs) have emerged as solutions to accelerate chemical and materials discovery research [1, 2, 3]. Automated methods are essential for these discovery pipelines as they require precise repeatability, high-throughputs, and continuous operation to explore meaningful volumes of high-dimensional materials search

spaces [4, 5, 6, 7], such as electrolytes [8, 9], polymers [10, 11], and perovskites [12, 13]. SDLs and other robotic equipment are effective at automating time-consuming and repetitive tasks necessary for executing these experiments, while also improving task precision due to a coupled intelligent software-hardware control approach [4, 14, 5]. On the software end, computer vision and machine learning models collect and learn from data to improve the accuracy and precision of tasks within the materials discovery pipeline [15, 16, 17, 18]. Then, on the hardware end, automated pipettors and robotic arms execute those commands with high precision using those software outputs [4, 7, 6].

Robotic arms are widely used in SDLs for their reliability, precision, and speed [19, 20, 21, 7]. For example, robotic arms have been used in literature to automate materials preparation, synthesis, and characterization, including powder X-ray diffraction (XRD) [22], Reversible Addition-Fragmentation Chain-Transfer (RAFT) polymerization [23], and solid dispensing [24]. In combination with computer vision and fiducial markers, robotic arms use path planning to autonomously navigate to different positions for picking and placing of samples [25]. As part of a larger materials discovery pipeline, an important but often overlooked sub-task of an SDL is to replace a substrate that has been used to transfer and deposit materials onto for downstream characterization with a fresh, unused substrate for the next round of materials deposition [7, 26]. Without automation, this replacement process must be conducted *via* human intervention, bottlenecking the pipeline. Substrate types vary greatly across different materials and chemistry domains. For example, 96-well plates are used as substrates for aqueous pipetting of electrolytes or polymers [27, 28], metal alloyed plates are used as substrates for high-temperature sintered ce-

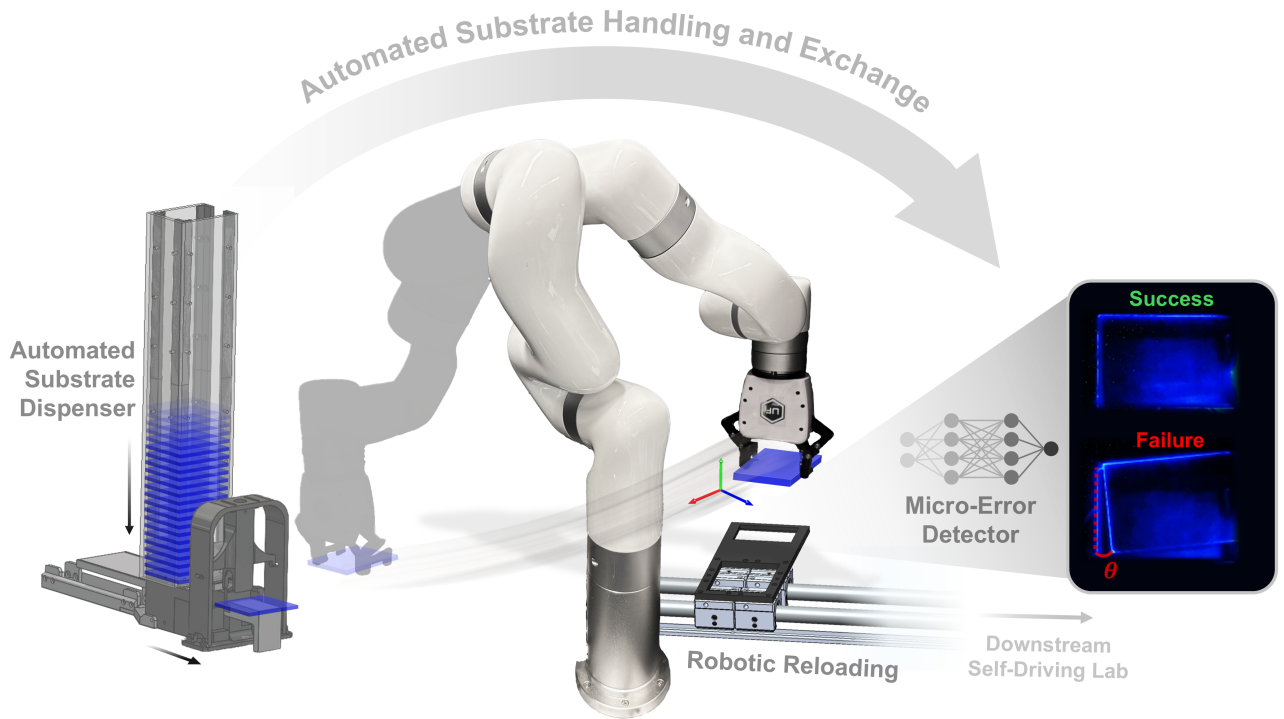


Figure 1: The Automated Substrate Handling and Exchange (ASHE) system for robotic manipulation and error correction of transparent substrate placement. ASHE combines the use of a dual-actuated dispenser, a 5-degree-of-freedom robotic arm with a specialized deformable gripper, and a deep learning computer vision detector to automate substrate reloading and unloading from experimental equipment. Through vision-based detection and automated correction of micro-scale errors in the placement of a substrate, ASHE carefully manipulates fragile and transparent substrates with high accuracy and repeatability, suited for the long, autonomous experimental campaigns of self-driving laboratories.

ramic coatings [29], and silica or glass slides are used as substrates for conductive carbon nanotubes or semiconductor perovskites [30, 31]. Robotic arms can be used to replace these substrates for the next cycle of an experiment. However, this task becomes significantly more challenging to perform autonomously with high accuracy and precision as the substrates become harder to detect and handle, *i.e.*, transparent, thin, and fragile glass or silica substrates, as often used in experiments with conductive materials [32, 30, 33, 31, 34, 35].

With the advancement of computer vision methods and machine learning-based image segmentation methods, such as You Only Look Once (YOLO) [36], Segment Anything Model (SAM) [37], and 3DSAM [38], object detection has greatly improved in both accuracy and speed. However, transparent object detection and segmentation within images and environments remains a key challenge for these models due to the difficulty in resolving the edges of these objects in ambient lighting and obscuration from reflections, background interference, and refraction-induced distortions [39, 40, 41]. There have been numerous approaches to improve the detection of transparent objects, which include both tra-

ditional computer vision methods and deep learning methods [42, 43, 44]. Wang *et al.* [45] develop a segmentation network architecture to address the challenge of capturing the texture characteristics of glass objects in images. Using this architecture, the authors demonstrate an improved performance in standard segmentation metrics such as mean absolute error, intersection union, weighted F-measure, and balanced error rate when compared to advanced glass segmentation methods such as MirrorNet [46], SAM [37], and Translab [41]. Guo-Hua *et al.* [47] propose a method that uses a combination of RGB, depth, and infrared images to address the difficulty in detecting transparent objects in different environments. Using this method, the author demonstrated the same accuracy in recognizing transparent objects as well as a 130% reduction in falsely recognizing non-transparent objects, compared to the methods developed by Lysenkov *et al.* [48]. Although these approaches address certain limitations in object segmentation and false recognition of transparent objects, they do not directly translate to the detection of transparent substrates in SDLs, as these existing methods largely focus on 3D and curved glass objects, such as beakers

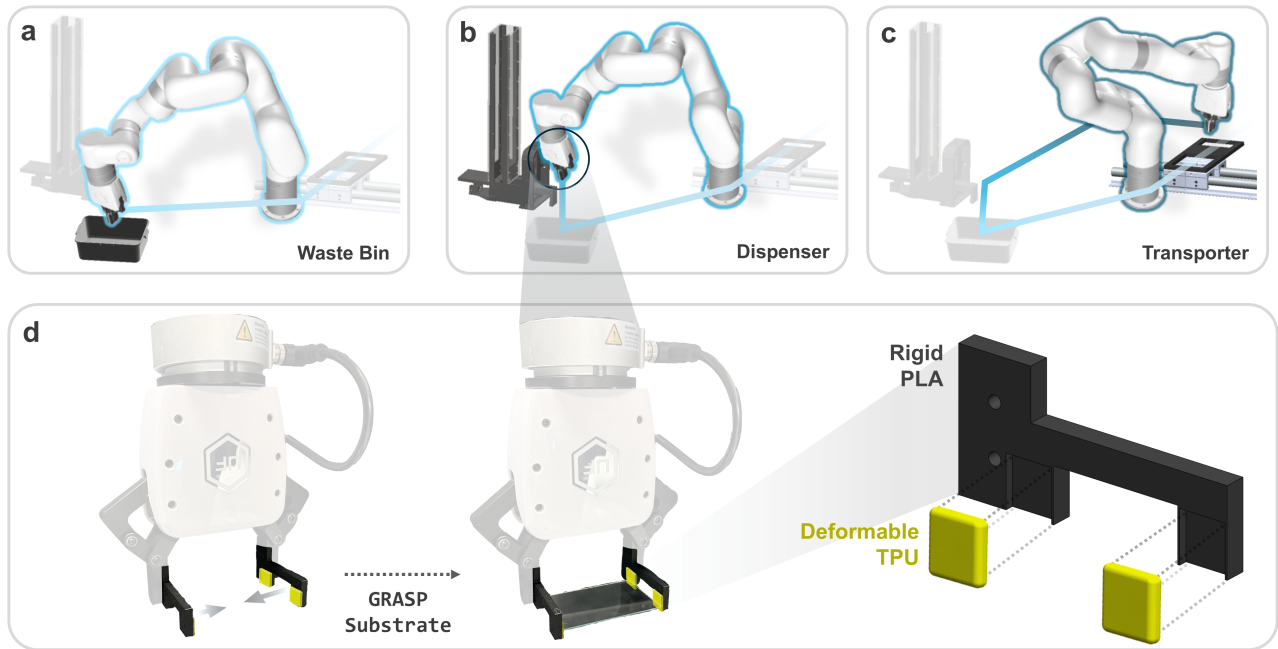


Figure 2: Robotic path plan for substrate reloading and grasping using specialized gripper fingers. The robotic arm path plan first (a) removes used substrates from the SDL transporter and moves them to a waste bin, then (b) picks up a fresh substrate from the dispenser, and finally (c) places the fresh substrate onto the SDL transporter. (d) Fragile substrates are manipulated with care, avoiding fracture through the use of a dual-material finger design that employs both rigid polylactic acid (PLA) and deformable thermoplastic polyurethane (TPU). Four points of contact are made between the substrate and the deformable TPU to ensure a secure grasp during robot motion.

and flasks, allowing the models to take advantage of warping and distortion for easier detection. Transparent substrates used for materials experiments are often thin and flat with no curvature for these models to hone in on. Although there have been a few studies that combine computer vision and deep learning methods to find a balance between accuracy and speed for general object detection [49, 50, 51], the literature is sparse on demonstrating generalizability to transparent object detection. Rani *et al.* [50] use traditional computer vision techniques to strip down an image before feeding its wireframe into a Fast Region-based Convolutional Network (Fast R-NN) model for object detection and classification purposes. Using this methodology, the authors demonstrated improved accuracy with faster computation, compared to existing techniques. Pulli *et al.* [52] apply pre-processing techniques to images passed through a convolutional neural network for improved detection of transparent objects only using RGB images. Promising results using this approach are demonstrated on a user-trained GDR-Net [53] framework, but the approach fails to improve performance using publicly accessible and pre-trained high-performance object detection models, such as YOLOX [54], limiting its generalizability. From these existing methods in the literature, joint computer vision and machine learning mod-

els for object detection have emerged as optimal architectures for improving general object detection accuracy and speed. However, further refinements and developments in these models are still required to reliably translate the methods to the detection of nearly featureless thin and flat transparent substrates for use within SDLs.

Responding to this research gap, we propose a robotic approach of Automated Substrate Handling and Exchange (ASHE) of transparent substrates within SDLs that combines computer vision and deep learning for reliable substrate manipulation and error correction. ASHE utilizes a coupled hardware-software control approach to accurately and repeatably detect the placement of transparent substrates, precisely and carefully manipulate them, and then determine and correct any placement failures in a closed-loop, as shown in Figure 1. On its hardware end, ASHE is equipped with a 5-degree-of-freedom (DOF) robotic arm, a specialized deformable gripper, and a dual-actuated dispenser to handle thin and fragile substrates. While on its software end, ASHE utilizes a fused geometric and deep learning model to reliably classify failed or successful transparent substrate placements by the robotic arm using lateral illumination techniques. With ASHE, we demonstrate a 98.5% first-time success rate in the fully automated pick-and-place of fragile, transparent substrates across 130 experimen-

tal reload cycles of an SDL for materials discovery.

2 Methods

ASHE consists of three primary components: a robotic arm and gripper, an actuated substrate dispenser, and a deep learning error detection model. Each of these components interacts synchronously to remove the used transparent substrates from a holder within an SDL that transports the substrate between subsystems (here, we call it a *transporter*), followed by dispensing and placing a new substrate on that transporter. Once placement has been completed, ASHE confirms if the new substrate has been placed successfully, and otherwise performs corrective re-positioning. Through a centralized integration of mechanical, electrical, and software systems, ASHE is commanded *via* updates to a Structured Query Language (SQL) database, enabling modular integration into the existing architecture of an SDL wirelessly or through wired serial communication.

2.1 Robotic Path Planning and Manipulation

ASHE uses the UFACTORY xArm 5, a 5-DOF robotic arm, chosen for its Python compatibility, cost-effectiveness, and positional repeatability of 0.1 mm, which is important for the reliable grasping of fragile substrates. Programmed path plans of the robotic arm and subsequent substrate manipulations are activated using a leader-follower control approach, as dictated by updates to a binary SQL database. Hence, ASHE remains idle while the SDL state variable in the SQL database is set to a 0. To initiate ASHE, the transporter of the SDL moves to its target position and depresses a limit switch, sending a signal to the SQL database to change the SDL state variable to a 1, which then activates ASHE’s path plan and concurrently dispenses a fresh substrate from the dual-actuated dispenser. First, the arm removes any used substrates from the SDL transporter and disposes them into a hazardous waste bin, as shown in Figure 2a. Second, the arm moves to the dispenser to grasp a fresh substrate, as shown in Figure 2b. Third, the arm moves to the transporter to place the fresh substrate, as shown in Figure 2c, where computer vision is then used to determine if the placement was successful.

To perform safe and successful grasping of fragile and brittle substrates such as glass and silica, a UFACTORY xARM gripper with custom-designed fingers is used for millimeter-scale control over the stroke and speed of the gripper actuation. Vacuum grippers were avoided since

they make contact with the top of the substrates rather than the sides. Contacting the top of the substrate results in potential damage to the vacuum seal over time from the materials and chemicals deposited onto them by the SDL as well as the vacuum gripper interfering with any coatings applied to the fresh substrates. These custom-designed fingers are 3D printed and employ a dual-material design, combining polylactic acid (PLA) and thermoplastic polyurethane (TPU), to overcome the difficulty of grasping fragile substrates, as shown in Figure 2d. Rigid PLA is used to provide structural integrity to the length of the finger for positioning precision, while deformable TPU 95A is used at the finger tips, providing compressibility during grasping contact to avoid fracture. We note that fingers with four points of contact on the sides of the substrate improve grasping when using deformable TPU tips, ensuring a more stable and secure grasp.

2.2 Dual-actuated Substrate Dispenser

The dual-actuated substrate dispenser allows for ASHE to operate during long self-driving experimental campaigns by dispensing fresh substrates from a tall stack that can hold over 300 glass substrates of size 50.8 mm \times 76.2 mm \times 1.0 mm, while maintaining certain substrate surface treatments such as hydrophobic Teflon coating. Using a dual actuator design, this structure dispenses fresh substrates automatically, adhering to the same leader-follower control scheme as the robotic arm. This subsystem is controlled by an Arduino Due microprocessor with L293D motor drivers to control the positions of both linear actuators that dispense the substrates from the stack.

Figure 3 illustrates a cross-sectional view of the dispensing procedure. A vertical hotel stores a tall stack of fresh substrates, enabling the subsystem to have a small footprint. Within this hotel, the lower-most substrates rest atop a 3D printed transfer plate attached to the horizontally positioned linear actuator. This transfer plate is designed with a small lip approximately 0.2 mm thinner than the thickness of each substrate, enabling it to push only the lower-most substrate out from the hotel during actuation, even with the weight of the substrates above, as shown in Figure 3a. When the horizontal actuator reaches its desired position, it depresses a limit switch, sending an electrical signal to activate a vertical actuator downward, as shown in Figure 3b. This vertical actuator extends a 3D printed wall into the return path of the transfer plate’s retraction to block the substrate from transferring back into the hotel, as shown in Fig-

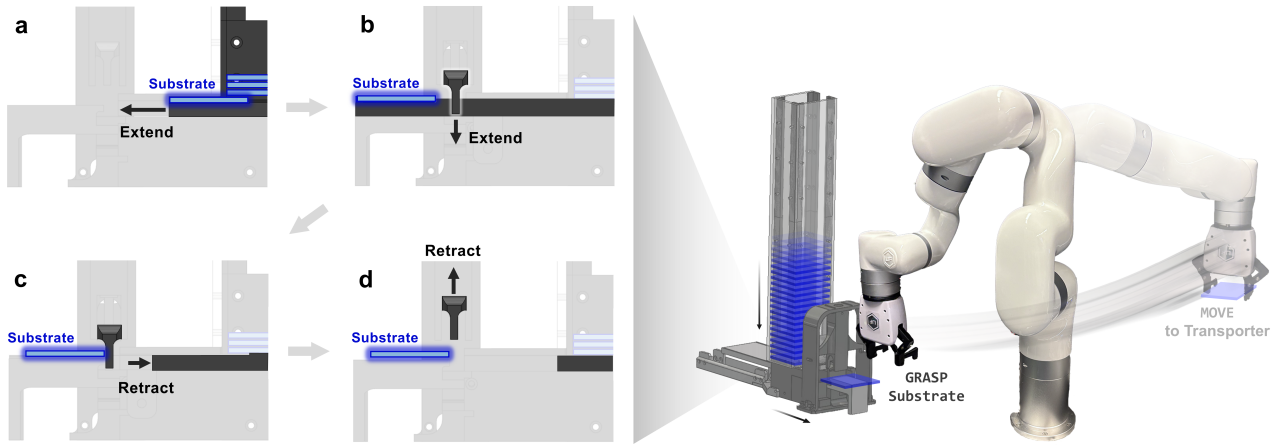


Figure 3: Dual-actuated dispenser sets fresh substrates for the robotic arm to grasp and move. (a) A single substrate is pushed from the bottom of a stack using horizontal actuation. (b) At the horizontal actuator’s full extension, a vertical actuator is released to block the substrate from reentry. (c) The substrate stays in place as the horizontal actuator retracts. (d) The vertical actuator retracts, leaving the substrate in place for the robotic arm to grasp.

ure 3c. Finally, once the horizontal actuator is retracted, then the vertical actuator retracts and the system is back in its initial state, ready for its next command, as shown in Figure 3d. The singular substrate now remains positioned on a platform to be picked up by the robotic arm for placement into the transporter of an SDL.

2.3 Transparent Substrate Detection

Misplacing a substrate onto a target position of an SDL will result in a cascade of failures downstream, such as misaligned material dispensing or coating and erroneous characterization measurement readings. Thus, it is imperative that the substrates be placed correctly into this target position, such as the target slot of the transporter. In this paper, we focus on the detection of transparent substrates useful for conductive materials experimentation, as this gap has not yet been addressed in the literature. However, detection of transparent substrates is a challenging task due to the difficulty of resolving their edges in ambient lighting, as shown in Figure 4a. Here, we circumvent many of these issues by using a method of laterally illuminating the transparent substrate from the side with blue light in the dark. Figure 4b illustrates the use of lateral illumination to strongly illuminate a blue boundary around the edges of the substrate through the refraction and diffusion of blue light within the substrate. This blue edge improves computer vision detection of the substrate position, enabling more accurate and robust detection of placement errors, as shown in Figure 4c.

ASHE uses an Intel RealSense D435 camera to image the blue light-illuminated transparent substrates as

placed into the transporter by the robotic arm. To detect whether the substrate has been successfully placed into the transporter, we propose a fused computer vision model approach. The first model uses the segmented geometry of the substrate compared to the target slot of the transporter to determine larger macro-scale errors in placement. The second model uses a deep learning convolutional neural network to determine smaller micro-scale errors in placement. Figure 5 shows the decision tree of the fused model approach that enables robust and high-accuracy failure detection of transparent substrate placements. If either model detects a failed placement, then the robotic arm executes its auto-correction plan of removing the misplaced substrate and placing a freshly dispensed one, as previously shown in Figure 2a–c.

2.3.1 Geometric Detection of Macro-scale Errors

The first part of the fused placement detection model for transparent substrates is a geometry-based computer vision model. This geometric model (GM) detects large placement errors by comparing the computed edges of both the target slot in the transporter and the transparent substrate. Figure 6a illustrates this placement detection procedure of the GM.

First, the edges of the target slot in the transporter are detected. An image of the initial empty transporter is captured from the live feed of the aerial RealSense D435 before substrate placement. This image is then gray-scaled and blurred with a Gaussian filter to suppress noise in the surface texture. Then, Canny edge detection with a wide hysteresis threshold (30, 300) is performed [55]. The large upper threshold isolates strong struc-

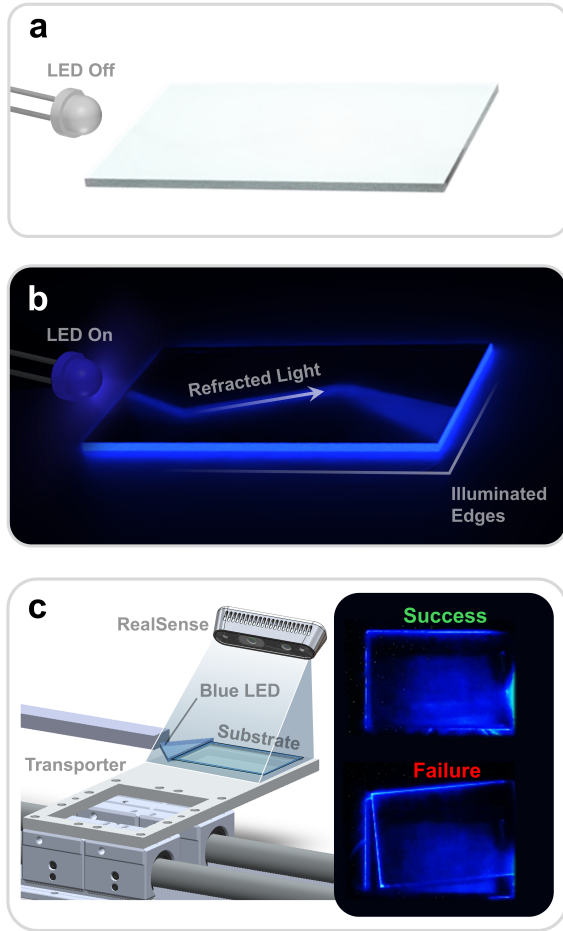


Figure 4: Lateral illumination of transparent substrates using blue light for computer vision detection. (a) Rendering of a transparent glass substrate in ambient light with no lateral illumination. (b) Rendering of a transparent glass substrate in the dark with blue light lateral illumination. The light refracts within the glass and emits along the edge faces of the substrate, illuminating them for clearer computer vision detection. (c) The computer vision imaging setup with RealSense D435 camera and lateral blue light illumination used for error detection in transparent substrate placement. Experimental images are shown of a transparent glass substrate successfully and unsuccessfully placed into the target slot of the transporter under the lateral illumination condition.

tural boundaries, while the small lower threshold keeps relevant faint edges to account for uneven lighting conditions and shadows introduced by the blue light. Noisy edges are pruned if they do not meet a length threshold of at least 100 pixels. Finally, disconnected edges are closed by enforcing the known rigid geometry of the transporter using a convex hull transformation [56], fitting the detected edges to a bounding rectangle.

Second, the edges of the placed transparent substrate are detected. This vision system takes advantage of the high-contrast lateral blue light illumination diffusely emitted from the edge faces of the substrate to perform

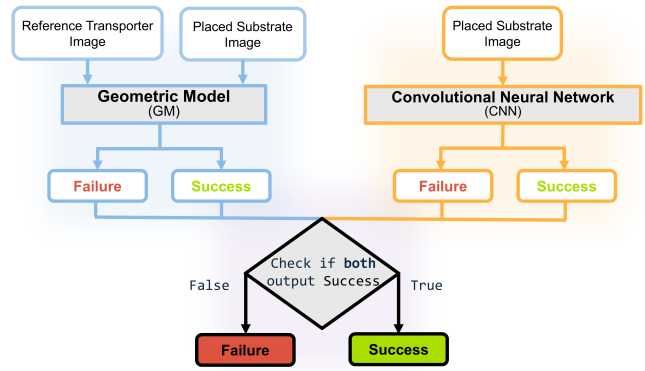


Figure 5: Fused geometric model (GM) and convolutional neural network (CNN) decision tree for reliable classification of placement errors for transparent substrates. A successful placement is declared only if the GM and CNN both output `success` classifications of the substrate placement.

edge detection. After robotic placement onto the transporter, a picture of the substrate is captured from the same reference frame as the initial empty transporter image using the aerial RealSense D435 camera. This image is blurred and filtered using a blue color mask to enhance the contrast around the edges of the substrate, which is then followed by Canny edge detection [55]. Using Canny edge detection on the color-masked image generates fragmented edges, resulting in inconsistent bounding rectangle results. Thus, a Hough transform [57] is used to compute straight lines from the edge image. Finally, similar to determining the edges of the target slot in the transporter, the substrate edge segments are aggregated, approximated into a polygon, and bound to a convex hull [56] to construct the final bounding rectangle of the transparent substrate.

This segmentation process is repeated across 100 sampled frames taken from the RealSense D435 camera for both the target transporter slot and the transparent substrate to account for noise in the image and the scene in classifying placement success. Using the known approximate pixel dimensions of both the slot and substrate, only appropriately sized bounds are kept across these 100 computations. The average bounds of both the slot and the substrate are then computed and compared using Shapely [58] to calculate the overlap percentage and relative rotation mismatch. A failed placement is output by the GM if shapes have either an area overlap of less than 90%, determined through empirical testing. If the GM outputs a `failure` placement classification, then the robotic arm executes its auto-correction plan of removing the misplaced substrate and placing a freshly dispensed one, as previously shown in Figure 2a–c.

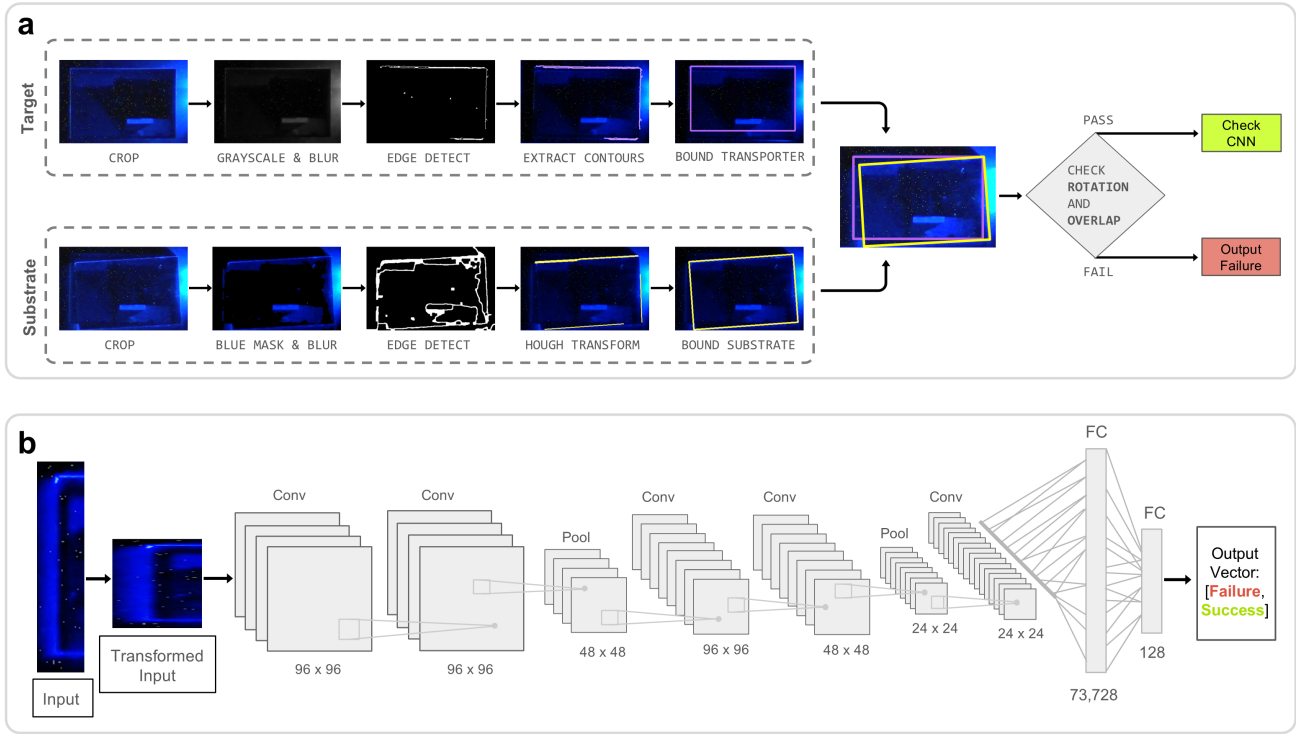


Figure 6: Workflow diagrams for the (a) geometric model (GM) and the (b) convolutional neural network (CNN) used for the detection of placement errors of transparent substrates. (a) The GM compares the bound edges created from both the placed substrate under lateral illumination and the target slot of the SDL transporter, where the substrate should be placed. Bound edges are formed through a suite of transformations, including color masking, edge detection, Hough transform, and convex hull transforms. If the reference and substrate bounding areas achieve an overlap greater than 90%, then the GM outputs a `success` and checks the CNN for a corresponding `success`. (b) The CNN uses only one full edge and two partial edges of a laterally illuminated substrate image to classify the success of a placement. An image input to the CNN is reshaped into size 96×96 and passed through two 2D convolutional layers using 32 filters with 3×3 kernels. After max pooling, the feature map is passed through two more 2D convolutional layers using 64 filters with 3×3 kernels each, followed by a second max pooling. The fifth and final convolution uses 128 filters with a 3×3 kernel. The resulting feature map is flattened to a 1D vector and processed by a classification head with two fully connected layers and a 50% dropout layer after the first fully connected layer to prevent overfitting. The CNN outputs a vector of length 2, where each output corresponds to the confidence of either a `failure` or a `success` classification, respectively $\in [0, 1]$.

2.3.2 Deep Learning Detection of Micro-scale Errors

The second part of the fused placement detection model for transparent substrates is a 2D convolutional neural network (CNN). This CNN detects small placement errors through training on a labeled dataset of various rotational and translational placement errors. The collected dataset consists of 1990 captured images (996 unique failure cases and 994 success cases), prior to augmentation. For accurate micro-error detection, the raw RGB color is preserved for model training, and the images are cropped from 1920×1080 pixels into a fixed region of interest of 380×250 pixels along the far edge of the substrate from the blue LED. We note this cropping procedure improves CNN model performance by zooming in on regions containing more dense information on substrate placement accuracy and removes dead zones in the center of the substrate that provide little information

on substrate position. Data augmentation was applied to improve model robustness to minor environmental changes in the input and to ensure the model could be generalized. These data augmentations included random shifts (± 5 pixels), rotations (± 1 degree), zooms ($\pm 2\%$), brightness adjustment (± 10), contrast adjustment ($\pm 5\%$), and Gaussian noise (± 5), generating 15 mutations per image, resulting in a total dataset size of 29,850 images. These augmentation values were selected to mimic realistic mechanical tolerances and sensor noise without changing key characteristics of the imaged substrate placement error. The dataset is split into 80% training and 20% validation subsets before augmentation to prevent data leakage. A weighted cross-entropy loss function was implemented to account for the data imbalance between success images and augmented failure images, reducing the rate of false positives by increasing attention to the minority class during

model training. The model was trained using a learning rate of 1×10^{-3} with a batch size of 32 over 50 epochs. Early stopping was implemented to prevent overfitting and to produce final model weights with the highest validation accuracy.

A shallow CNN architecture was created in PyTorch [59] to learn micro-scale placement errors of the transparent substrates within the transporter under lateral illumination of blue light. Figure 6b illustrates the micro-error detection CNN architecture designed for this study. The CNN architecture was designed to preserve spatial distribution during the early extraction of features, enabling the model to capture subtle spatial dependencies using the early feature maps. The network accepts a three-channel input tensor of 96×96 pixels (reshaped from the cropped 380×250 raw RGB image) and outputs a vector of length 2 from a classification head, where each output represents the classification confidence of a failure and success, respectively. During test time, ASHE utilizes the model to classify placement success with a confidence score across 100 uniquely sampled frames from the RealSense D435 camera live stream, returning the median placement success score. The placement success score is derived from the CNN’s prediction confidence and is fitted onto a likelihood scale ranging from 0 (failure) to 1 (success). If the median achieves a placement success score of over 60%, then the CNN part of the fusion model classifies the placement as a `success`. The placement success score threshold of 60% was chosen after empirically testing various minuscule rotational and translation errors in substrate placement. If the CNN classifies the placement as a `failure`, then ASHE prompts the robotic arm to execute its auto-correction plan of removing the misplaced substrate and placing a freshly dispensed one, as previously shown in Figure 2a–c.

3 Results

3.1 Transparent Substrate Vision Detection Performance

Using the fused GM-CNN model, we demonstrate that reliable detection of transparent substrate placement failures is achieved across an array of realistic error modes. The GM is used as the initial rejection model for large, obvious errors, while the CNN is used to determine small errors nearly imperceptible to the human eye. However, a successful placement is not confirmed unless the GM and CNN both classify the placement as a `success`.

Figure 7 illustrates both the GM and CNN model performance across 36 unique transparent glass substrate placement errors, including small, medium, and large errors in both translation and rotation. From these results, we highlight that the GM and CNN perform similarly on both rotational errors and translational errors. However, dramatic performance differences between the models can be seen across the small, medium, and large errors. For rotation, *small errors* in substrate placement have an angle mismatch with the target transporter slot of less than approximately 1.7° , while *large errors* have an angle mismatch greater than approximately 5.4° . For both horizontal and vertical translation, *small errors* in substrate placement have a displacement less than approximately 2.4 mm, while *large errors* have a displacement greater than approximately 5.6 mm.

In Figure 7, the placement success classifications for both the GM and CNN models are shown above every image. The GM correctly detects $\frac{19}{20}$ of the large errors with only one false positive that has a counter-clockwise rotational error of 1.8° and a translational error of 2.7 mm. The CNN correctly detects all $\frac{20}{20}$ of the large errors with a prediction confidence of 100% for all 20 large error images. Moving into the medium errors, the GM correctly detects $\frac{0}{12}$ of the medium errors, outputting false positives for all 12 images. The CNN correctly detects all $\frac{12}{12}$ of the medium errors with a prediction confidence ranging from 97% to 100%. Lastly, for the small errors, the GM correctly detects $\frac{0}{4}$ of the small errors, outputting false positives for all 4 images. The CNN correctly detects all $\frac{4}{4}$ of the small errors with a prediction confidence ranging from 99% to 100%. Both the GM and CNN correctly classify a `success` for the successful placement image.

3.2 ASHE Repeatability Performance

Combining the robotic arm with specialized deformable grippers, the dual-actuated substrate dispenser, and the fused GM-CNN vision detection model, we experimentally validate the performance of the complete closed-loop ASHE pipeline. In these experiments, each trial represents an independent reloading procedure performed by ASHE, activated through the leader-follower control approach when the SDL transporter reaches its reloading position and depresses a limit switch, changing its SQL state variable from 0 to 1, in turn commanding ASHE to begin the reloading procedure. Figure 8 shows the results of these repeatability experiments running on the complete ASHE system.

Figure 8a highlights the closed-loop failure detection

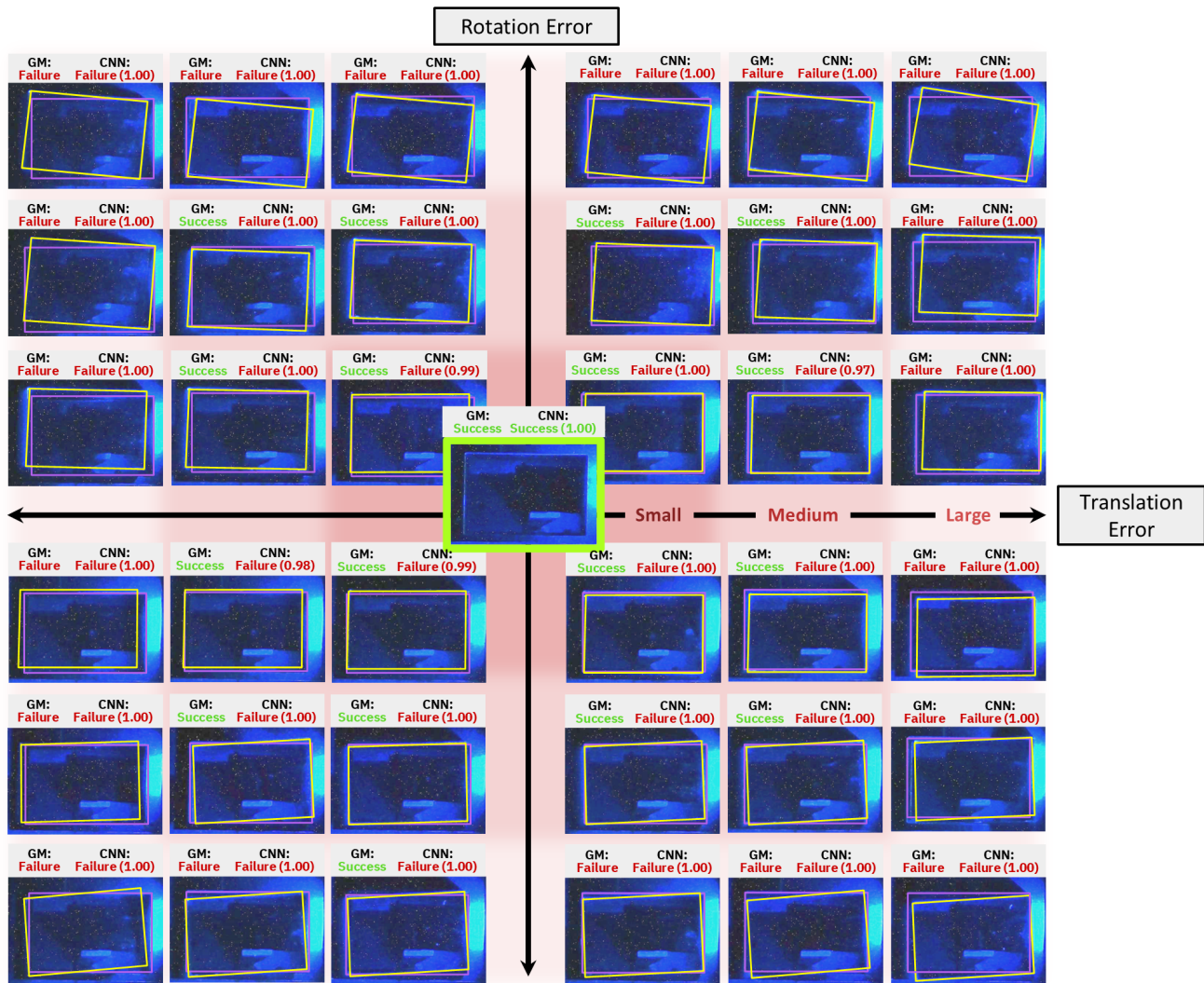


Figure 7: Transparent substrate placement error detection results of the geometric model (GM) and convolutional neural network (CNN) across an array of 36 unique placement error types and magnitudes. Each image within the matrix represents a unique placement error of a transparent substrate illuminated laterally by blue light. The yellow rectangle within each image represents the ground truth position of the substrate, while the purple rectangle represents the ground truth position of the SDL transporter target slot. Along the X-axis of the matrix, translational errors in placement increase in magnitude moving away from the center origin. Along the Y-axis of the matrix, rotational errors in placement increase in magnitude moving away from the center origin. The outermost ring of 20 images in the matrix represents placement errors with large translational and/or rotational errors. The middle ring of 12 images in the matrix represents placement errors with medium translational and/or rotational errors. The inner ring of 4 images in the matrix represents placement errors with small translational and/or rotational errors. The innermost image represents a successful placement. The output GM and CNN classifications are indicated above each image, along with the CNN classification confidence for that image. The yellow and purple bounding rectangles are for visualization purposes only and are not present in the raw data passed to the models for classification.

and auto-correction capabilities of ASHE on 10 pre-programmed robotic arm substrate placement failures. The dark red open scatter points indicate ASHE's first attempt at placement into the SDL transporter, which are pre-programmed to fail, and, here, ASHE correctly classifies $\frac{10}{10}$ as failure. The light green solid scatter points indicate ASHE's second placement attempt to correct these detected failures of the first attempt. We demonstrate that $\frac{10}{10}$ of the automated corrective procedures successfully corrected the placement failures on

the second placement attempt, resulting in success classifications by the vision system.

Figure 8b demonstrates the long-form automated reliability and repeatability performance of ASHE across 130 uniquely commanded reloading procedures, without any pre-programmed failures. ASHE classifies success placements on $\frac{128}{130}$ of the reload cycles on the first attempt. For every placement, a human domain expert monitors the placement result, and all $\frac{128}{130}$ are validated as correctly classified. Therefore, across these 130

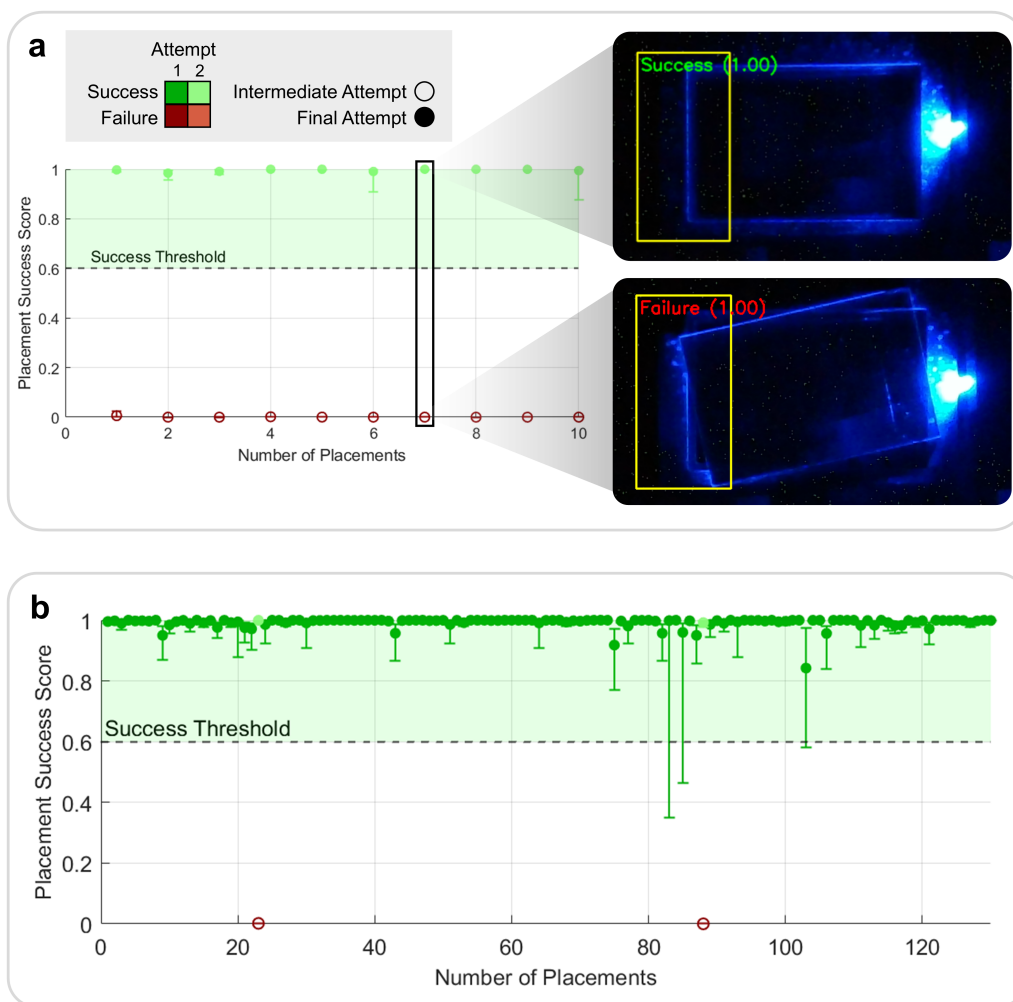


Figure 8: Experimental results of the closed-loop ASHE system reloading transparent glass substrates within an SDL. (a) Computer vision error detection and correction performance of ASHE across 10 pre-programmed failures in robotic arm placement of transparent substrates. (b) Long-form repeatability tests across 130 independent cycles of transparent glass substrate pick-and-placement using ASHE, without pre-programmed failures. Each scatter point represents a placement success score of a freshly dispensed substrate into the target slot of an SDL transporter by the robotic arm. The placement success score is derived from the CNN’s prediction confidence and is fitted onto a likelihood scale ranging from 0 (failure) to 1 (success). An empty scatter point represents an intermediate attempt at placement, while a full scatter point represents the final attempt at placement. The shade of these scatter points represents the placement attempt: a darker shade for the first placement attempt and a lighter shade for the second placement attempt. The color of the scatter point represents the median confidence score of the fused GM-CNN model, with error bars illustrating the 25th and 75th percentiles across 100 predictions, each on a unique frame taken from the RealSense D435 camera live stream after placement. For every trial, the vision classification is validated by a human domain expert to correctly match the real-world failure or successful placement.

experiments, ASHE achieves a 98.5% first-time placement accuracy. ASHE classifies the remaining $\frac{2}{130}$ substrates as *failure*, which are validated by the human domain expert. Upon this *failure* classification, ASHE automatically corrects the failures and places fresh substrates, classifying these second attempts as *success*, which are validated by the human domain expert. Ultimately, through the closed-loop detection and auto-correction capabilities of ASHE, 100% of the substrates are placed correctly into the target slot of the SDL transporter by the second attempt. These results are

noted to transfer to transparent substrates with various non-streaking and transparent surface treatments, such as hydrophobic Teflon coatings and hydrophilic plasma treatments.

4 Discussion and Conclusions

In this current expansion of automated methods for materials discovery and self-driving laboratories [3, 7, 9], improving system accuracy and repeatability is important to further the advancement and success of these lab-

oratories. With the foundation of materials and chemical sciences starting with a substrate to transfer or dispense materials onto [60], it is critical that the infrastructure of these self-driving laboratories be developed to handle and manipulate a wide variety of substrates with high accuracy and repeatability. The most challenging substrates for automated methods to manipulate are fragile, thin, and transparent substrates, such as glass or silica, used for conductive materials [32, 30, 33, 31, 34, 35], since current methods fail to detect or sufficiently generalize to these nearly featureless substrates [42, 43, 44]. Thus, a research gap exists in designing software capabilities to accurately detect these transparent substrates as well as hardware capabilities to reliably manipulate them, while automatically correcting for failed placements.

In this paper, we present a fully closed-loop system for automating transparent substrate handling and exchange in self-driving laboratories, entitled ASHE. ASHE synchronously integrates a 5-degree-of-freedom robotic arm with a specialized deformable gripper, a dual-actuated substrate dispenser, and a fused geometric and deep learning vision detection model to accurately unload used substrates and load fresh substrates with full automation within a self-driving laboratory. The fused geometric and deep learning vision system in ASHE enables micro-scale error detection and closed-loop correction of substrate misplacements. In this paper, we show that the fused model approach accurately classifies small, medium, and large translational and rotational placement errors of transparent substrates with classification confidence ranging from 97% to 100%. We run 130 independent trials of ASHE reloading substrates into a self-driving laboratory and demonstrate 98.5% first-time placement accuracy, validated by a human domain expert, with only two substrate misplacements. ASHE automatically detects these misplaced substrates and automatically corrects their placements.

We demonstrate that ASHE is robust to false positives and tends to overgeneralize classifications of successfully placed substrates as *failure* instead. This behavior is advantageous as it mitigates the risk of passing a misplaced substrate through to the self-driving laboratory, which would likely result in a cascade of downstream failures if the substrate is not properly set into its target position. False negatives are preferable to encounter using ASHE compared to the alternative false positive, since the automated error correction mechanism is implemented to handle these instances by automatically activating reloading protocol upon a *failure* classification.

Although ASHE demonstrates promising performance results towards the advancement of automated transparent substrate manipulation, vision detection, and error correction, several limitations exist in its generalizability. Specifically, the hardware and software components of the system have been designed and trained to perform highly on glass substrates of a particular size of 50.8 mm \times 76.2 mm \times 1.0 mm. To extend the use of ASHE to substrates outside of these parameters, the actuated substrate dispenser and gripper fingers must be redesigned, and the deep learning model must be retrained on a newly collected dataset for that particular substrate. Furthermore, wider adoption of the technologies used to develop ASHE may be inhibited by their costs. Although many of the components of ASHE are 3D printed, the main cost sinks include the UFACTORY xARM 5 at \$6000 USD, and its corresponding gripper at \$2300 USD. While these costs are on the lower end of robotic arms, acquiring hardware with sufficient precision capabilities governs the overall success of the system.

Ultimately, ASHE helps to close the research gap in fragile and transparent substrate manipulation. Through the integration of robotic arms, automated substrate dispensing, and reliable vision detection, closed-loop control and error correction are established. With ASHE, we move towards an improvement in the automation capabilities of self-driving materials laboratories with accurate, reliable, and robust robotic manipulation for fragile and transparent substrates.

Author contributions

A.E.S. and T.B. conceptualized the work. K.F. and A.E.S. designed the methodology. K.F., I.G., and A.E.S. designed and built the hardware and electronics. K.F. and A.G. wrote the software. K.F., A.G., and I.G. conducted experiments. K.F., A.G., and A.E.S. wrote the manuscript. All authors reviewed and edited the manuscript. A.E.S. and T.B. provided guidance.

Conflicts of interest

There are no conflicts to declare.

Data availability

The code and data presented in this article are available on GitHub at <https://github.com/PV-Lab/ASHE>.

Acknowledgements

The authors acknowledge the support of the Massachusetts Institute of Technology Undergraduate Research Opportunities Program (UROP) office and the MIT Energy Initiative (MITEI) program. The authors acknowledge Eunice Aissi and Alexander Love for their fruitful discussions on system design modifications and improvements.

References

- [1] Milad Abolhasani and Eugenia Kumacheva. The rise of self-driving labs in chemical and materials sciences. *Nature Synthesis*, 2(6):483–492, 2023.
- [2] Alexander V. Tobias and Adam Wahab. Autonomous ‘self-driving’ laboratories: a review of technology and policy implications. *Royal Society Open Science*, 12(7):250646, 2025.
- [3] Gary Tom, Stefan P. Schmid, Sterling G. Baird, Yang Cao, Kouros Darvish, Han Hao, Stanley Lo, Sergio Pablo-García, Ella M. Rajaonson, Marta Skreta, Naruki Yoshikawa, Samantha Corapi, Gun Deniz Akkoc, Felix Strieth-Kalthoff, Martin Seifrid, and Alán Aspuru-Guzik. Self-driving laboratories for chemistry and materials science. *Chemical Reviews*, 124(16):9633–9732, 2024.
- [4] Jackie T. Yik, Leiting Zhang, Jens Sjölund, Xu Hou, Per H. Svensson, Kristina Edström, and Erik J. Berg. Automated electrolyte formulation and coin cell assembly for high-throughput lithium-ion battery research. *Digital Discovery*, 2:799–808, 2023.
- [5] Kazunori Nishio, Akira Aiba, Kei Takihara, Yota Suzuki, Ryo Nakayama, Shigeru Kobayashi, Akira Abe, Haruki Baba, Shinichi Katagiri, Kazuki Omoto, Kazuki Ito, Ryota Shimizu, and Taro Hito-sugi. A digital laboratory with a modular measurement system and standardized data format. *Digital Discovery*, 4:1734–1742, 2025.
- [6] Nathan J. Szymanski, Bernardus Rendy, Yuxing Fei, Rishi E. Kumar, Tanjin He, David Milsted, Matthew J. McDermott, Max Gallant, Ekin Dogus Cubuk, Amil Merchant, Haegyeom Kim, Anubhav Jain, Christopher J. Bartel, Kristin Persson, Yan Zeng, and Gerbrand Ceder. An autonomous laboratory for the accelerated synthesis of novel materials. *Nature*, 624:86–91, 2023.
- [7] B. P. MacLeod, F. G. L. Parlane, T. D. Morrissey, F. Häse, L. M. Roch, K. E. Dettelbach, R. Moreira, L. P. E. Yunker, M. B. Rooney, J. R. Deeth, V. Lai, G. J. Ng, H. Situ, R. H. Zhang, M. S. Elliott, T. H. Haley, D. J. Dvorak, A. Aspuru-Guzik, J. E. Hein, and C. P. Berlinguette. Self-driving laboratory for accelerated discovery of thin-film materials. *Science Advances*, 6(20):eaaz8867, 2020.
- [8] Murat Cihan Sorkun, Xuan Zhou, Joannes Murigneux, Nicola Menegazzo, Ayush Kumar Narsaria, David Thanoon, Peter A. A. Klusener, Kaustubh Kaluskar, Sharan Shetty, Efstathios Barmoutsis, and Süleyman Er. Redcat, an automated discovery workflow for aqueous organic electrolytes. *Digital Discovery*, 4:1844–1855, 2025.
- [9] George Crabtree. Self-driving laboratories coming of age. *Joule*, 4:2538–2541, 2020.
- [10] Stephen T. Knox, Kai E. Wu, Nazrul Islam, Roisin O’Connell, Peter M. Pittaway, Kudakwashe E. Chingono, John Oyekan, George Panoutsos, Thomas W. Chamberlain, Richard A. Bourne, and Nicholas J. Warren. Self-driving laboratory platform for many-objective self-optimisation of polymer nanoparticle synthesis with cloud-integrated machine learning and orthogonal online analytics. *Polym. Chem.*, 16:1355–1364, 2025.
- [11] Chengshi Wang, Yeon-Ju Kim, Aikaterini Vriza, Rohit Batra, Arun Baskaran, Naisong Shan, Nan Li, Pierre Darancet, Logan Ward, Yuzi Liu, Maria K. Y. Chan, Subramanian K.R.S. Sankaranarayanan, H. Christopher Fry, C. Suzanne Miller, Henry Chan, and Jie Xu. Autonomous platform for solution processing of electronic polymers. *Nature Communications*, 16(1):1498, 2025.
- [12] Sina Sadeghi, Karl Mattsson, Joshua Glasheen, Victoria Lee, Christine Stark, Pragyana Jha, Nikolai Mukhin, Junbin Li, Arup Ghorai, Negin Orouji, Christopher H. J. Moran, Alireza Velayati, Jeffrey A. Bennett, Richard B. Canty, Kristofer G. Reyes, and Milad Abolhasani. A self-driving fluidic lab for data-driven synthesis of lead-free perovskite nanocrystals. *Digital Discovery*, 4:1722–1733, 2025.

- [13] Jinge Xu, Christopher H. J. Moran, Arup Ghorai, Fazel Bateni, Jeffrey A. Bennett, Nikolai Mukhin, Koray Latif, Andrew Cahn, Pragyan Jha, Fernando Delgado Licona, Sina Sadeghi, Lior Politi, and Milad Abolhasani. Autonomous multi-robot synthesis and optimization of metal halide perovskite nanocrystals. *Nature Communications*, 16(1):7841, 2025.
- [14] Beatrice W. Soh, Aniket Chitre, Wen Yang Lee, Daniil Bash, Jatin N. Kumar, and Kedar Hippalgaonkar. Automated pipetting robot for proxy high-throughput viscometry of newtonian fluids. *Digital Discovery*, 2:481–488, 2023.
- [15] Thomas Pickles, Youcef Leghrib, Matt Weishaar, Mikhail Goncharuk, Peter Timperman, Timothy Doherty, David D. Ford, Jonathan Moores, Alastair J. Florence, and Cameron J. Brown. Automated scale-up crystallisation datafactory for model-based pharmaceutical process development: a bayesian case study. *Digital Discovery*, 4:2025–2032, 2025.
- [16] Hengrui Zhang, Tianxing Lai, Jie Chen, Arumugam Manthiram, James M. Rondinelli, and Wei Chen. Learning molecular mixture property using chemistry-aware graph neural network. *PRX Energy*, 3:023006, 2024.
- [17] Shiwei Lin, Zesen Chen, Xiaobin Jia, Yi Wang, Chenxu Wang, Shuyuan Zhang, Xiaozhen Ding, Boyuan Du, Weili Ding, and Huaping Liu. A Visual Dataset for Anomaly Detection in Self-Driving Laboratories. *Scientific Data*, 12(1):1787, 2025.
- [18] Riley J. Hickman, Malcolm Sim, Sergio Pablo-García, Gary Tom, Ivan Woolhouse, Han Hao, Zeqing Bao, Pauric Bannigan, Christine Allen, Matteo Aldeghi, and Alán Aspuru-Guzik. Atlas: a brain for self-driving laboratories. *Digital Discovery*, 4:1006–1029, 2025.
- [19] Oliver Bayley, Elia Savino, Aidan Slattery, and Timothy Noël. Autonomous chemistry: Navigating self-driving labs in chemical and material sciences. *Matter*, 7(7):2382–2398, 2024.
- [20] Benjamin Burger, Phillip M Maffettone, Vladimir V Gusev, Catherine M Aitchison, Yang Bai, Xiaoyan Wang, Xiaobo Li, Ben M Alston, Buyi Li, Rob Clowes, et al. A mobile robotic chemist. *Nature*, 583(7815):237–241, 2020.
- [21] Connor W Coley, Dale A Thomas III, Justin AM Lummiss, Jonathan N Jaworski, Christopher P Breen, Victor Schultz, Travis Hart, Joshua S Fishman, Luke Rogers, Hanyu Gao, et al. A robotic platform for flow synthesis of organic compounds informed by ai planning. *Science*, 365(6453):eaax1566, 2019.
- [22] Yuto Yotsumoto, Yusaku Nakajima, Ryusei Takamoto, Yasuo Takeichi, and Kanta Ono. Autonomous robotic experimentation system for powder x-ray diffraction. *Digital Discovery*, 3:2523–2532, 2024.
- [23] Jules Lee, Prajakatta Mulay, Matthew J. Tamasi, Jonathan Yeow, Molly M. Stevens, and Adam J. Gormley. A fully automated platform for photoinitiated raft polymerization. *Digital Discovery*, 2:219–233, 2023.
- [24] Ying Jiang, Hatem Fakhrudeen, Gabriella Pizzuto, Louis Longley, Ai He, Tianwei Dai, Rob Clowes, Nicola Rankin, and Andrew I. Cooper. Autonomous biomimetic solid dispensing using a dual-arm robotic manipulator. *Digital Discovery*, 2:1733–1744, 2023.
- [25] Chandima Fernando, Hailey Marcello, Jakub Wlodek, John Sinsheimer, Daniel Olds, Stuart I. Campbell, and Phillip M. Maffettone. Robotic integration for end-stations at scientific user facilities. *Digital Discovery*, 4:1083–1091, 2025.
- [26] Keiji Fushimi, Yusuke Nakai, Akiko Nishi, Ryo Suzuki, Masahiro Ikegami, Risa Nimura, Taichi Tomono, Ryota Hidese, Hisashi Yasueda, Yusuke Tagawa, and Tomohisa Hasunuma. Development of the autonomous lab system to support biotechnology research. *Scientific Reports*, 15(1):6648, 2025.
- [27] Shoichi Matsuda, Guillaume Lambard, and Keitaro Sodeyama. Data-driven automated robotic experiments accelerate discovery of multi-component electrolyte for rechargeable li–o₂ batteries. *Cell Reports Physical Science*, 3(4):100832, 2022.
- [28] Yang Bai, Liam Wilbraham, Benjamin J Slater, Martijn A Zwijnenburg, Reiner Sebastian Sprick, and Andrew I Cooper. Accelerated discovery of

- organic polymer photocatalysts for hydrogen evolution from water through the integration of experiment and theory. *Journal of the American Chemical Society*, 141(22):9063–9071, 2019.
- [29] X-J Lu and P Xiao. Constrained sintering of ysz/al₂o₃ composite coatings on metal substrates produced from electrophoretic deposition. *Journal of the European Ceramic Society*, 27(7):2613–2621, 2007.
- [30] Daniil Bash, Yongqiang Cai, Vijila Chellappan, Swee Liang Wong, Xu Yang, Pawan Kumar, Jin Da Tan, Anas Abutaha, Jayce JW Cheng, Yee-Fun Lim, et al. Multi-fidelity high-throughput optimization of electrical conductivity in p3ht-cnt composites. *Advanced Functional Materials*, 31(36):2102606, 2021.
- [31] Minsub Um, Sheryl L Sanchez, Hochan Song, Benjamin J Lawrie, Hyungju Ahn, Sergei V Kalinin, Yongtao Liu, Hyosung Choi, Jonghee Yang, and Mahshid Ahmadi. Tailoring molecular space to navigate phase complexity in cs-based quasi-2d perovskites via gated-gaussian-driven high-throughput discovery. *Advanced Energy Materials*, 15(16):2404655, 2025.
- [32] DB Fraser and HD Cook. Highly conductive, transparent films of sputtered in₂-xsnx o 3- y. *Journal of the Electrochemical Society*, 119(10):1368, 1972.
- [33] Yingjie Ma and Linjie Zhi. Graphene-based transparent conductive films: material systems, preparation and applications. *Small Methods*, 3(1):1800199, 2019.
- [34] Alexander E Siemenn, Eunice Aissi, Fang Sheng, Armi Tiihonen, Hamide Kavak, Basita Das, and Tonio Buonassisi. Using scalable computer vision to automate high-throughput semiconductor characterization. *Nature Communications*, 15(1):4654, 2024.
- [35] Shijing Sun, Armi Tiihonen, Felipe Oviedo, Zhe Liu, Janak Thapa, Yicheng Zhao, Noor Titan P Hartono, Anuj Goyal, Thomas Heumueller, Clio Batali, et al. A data fusion approach to optimize compositional stability of halide perovskites. *Material*, 4(4):1305–1322, 2021.
- [36] Joseph Redmon, Santosh Divvala, Ross Girshick, and Ali Farhadi. You only look once: Unified, real-time object detection, 2016.
- [37] Alexander Kirillov, Eric Mintun, Nikhila Ravi, Hanzi Mao, Chloe Rolland, Laura Gustafson, Tete Xiao, Spencer Whitehead, Alexander C Berg, Wan-Yen Lo, et al. Segment anything. In *Proceedings of the IEEE/CVF international conference on computer vision*, pages 4015–4026, 2023.
- [38] SAM 3D Team, Xingyu Chen, Fu-Jen Chu, Pierre Gleize, Kevin J Liang, Alexander Sax, Hao Tang, Weiyao Wang, Michelle Guo, Thibaut Hardin, Xiang Li, Aohan Lin, Jiawei Liu, Ziqi Ma, Anushka Sagar, Bowen Song, Xiaodong Wang, Jianing Yang, Bowen Zhang, Piotr Dollár, Georgia Gkioxari, Matt Feiszli, and Jitendra Malik. Sam 3d: 3dfy anything in images, 2025.
- [39] Po-Jen Lai and Chiou-Shann Fuh. Transparent object detection using regions with convolutional neural network. In *IPPR conference on computer vision, graphics, and image processing*, volume 2, 2015.
- [40] Dongsheng Han, Chaoning Zhang, Yu Qiao, Maryam Qamar, Yuna Jung, SeungKyu Lee, Sung-Ho Bae, and Choong Seon Hong. Segment anything model (sam) meets glass: Mirror and transparent objects cannot be easily detected. *arXiv preprint arXiv:2305.00278*, 2023.
- [41] Enze Xie, Wenjia Wang, Wenhai Wang, Mingyu Ding, Chunhua Shen, and Ping Luo. Segmenting transparent objects in the wild. In *European conference on computer vision*, pages 696–711. Springer, 2020.
- [42] May Phyo Khaing and Mukunoki Masayuki. Transparent object detection using convolutional neural network. In Thi Thi Zin and Jerry Chun-Wei Lin, editors, *Big Data Analysis and Deep Learning Applications*, pages 86–93, Singapore, 2019. Springer Singapore.
- [43] Ruoning Yu, Wenyi Ren, Man Zhao, Jian Wang, Dan Wu, and Yingge Xie. Transparent objects segmentation based on polarization imaging and deep learning. *Optics Communications*, 555:130246, 2024.
- [44] Chengyu Zheng, Ding Shi, Xuefeng Yan, Dong Liang, Mingqiang Wei, Xin Yang, Yanwen Guo,

- and Haoran Xie. Glassnet: Label decoupling-based three-stream neural network for robust image glass detection. *Computer Graphics Forum*, 41(1):377–388, 2022.
- [45] Hanfang Wang, Yi Chai, and Tao Tao. A novel transparent object detection approach based on boundary optimization. In Yuriy S. Shmaliy, editor, *8th International Conference on Computing, Control and Industrial Engineering (CCIE2024)*, pages 223–233, Singapore, 2024. Springer Nature Singapore.
- [46] Jinnan Yan, Trung-Nghia Le, Khanh-Duy Nguyen, Minh-Triet Tran, Thanh-Toan Do, and Tam V Nguyen. Mirrornet: Bio-inspired camouflaged object segmentation. *IEEE access*, 9:43290–43300, 2021.
- [47] Chen Guo-Hua, Wang Jun-Yi, and Zhang Ai-Jun. Transparent object detection and location based on rgb-d camera. *Journal of Physics: Conference Series*, 1183(1):012011, 2019.
- [48] Ilya Lysenkov, Victor Eruhimov, and Gary Bradski. Recognition and pose estimation of rigid transparent objects with a kinect sensor. *Robotics*, 273(273-280):2, 2013.
- [49] Anumol Mathai, Li Mengdi, Stephen Lau, Ningqun Guo, and Xin Wang. Transparent Object Reconstruction Based on Compressive Sensing and Super-Resolution Convolutional Neural Network. *Photonic Sensors*, 12(4):220413, April 2022.
- [50] Shilpa Rani, Deepika Ghai, and Sandeep Kumar. Object detection and recognition using contour based edge detection and fast R-CNN. *Multimedia Tools and Applications*, 81(29):42183–42207, December 2022.
- [51] Jinyu Wang, Yingna Li, and Wenxiang Chen. Detection of glass insulators using deep neural networks based on optical imaging. *Remote Sensing*, 14(20):5153, 2022.
- [52] Tessa Pulli, Peter Hönig, Stefan Thalhammer, Matthias Hirschmanner, and Markus Vincze. Enhancing transparent object pose estimation: A fusion of gdr-net and edge detection. *arXiv preprint arXiv:2502.12027*, 2025.
- [53] Gu Wang, Fabian Manhardt, Federico Tombari, and Xiangyang Ji. Gdr-net: Geometry-guided direct regression network for monocular 6d object pose estimation. In *Proceedings of the IEEE/CVF conference on computer vision and pattern recognition*, pages 16611–16621, 2021.
- [54] Zheng Ge, Songtao Liu, Feng Wang, Zeming Li, and Jian Sun. Yolox: Exceeding yolo series in 2021. *arXiv preprint arXiv:2107.08430*, 2021.
- [55] John Canny. A computational approach to edge detection. *IEEE Transactions on pattern analysis and machine intelligence*, (6):679–698, 2009.
- [56] Gary Bradski. The opencv library. *Dr. Dobb's Journal: Software Tools for the Professional Programmer*, 25(11):120–123, 2000.
- [57] Dana H Ballard. Generalizing the hough transform to detect arbitrary shapes. *Pattern recognition*, 13(2):111–122, 1981.
- [58] Sean Gillies, Casper van der Wel, Joris Van den Bossche, Mike W. Taves, Joshua Arnott, Brendan C. Ward, et al. Shapely, 2025.
- [59] Adam Paszke, Sam Gross, Francisco Massa, Adam Lerer, James Bradbury, Gregory Chanan, Trevor Killeen, Zeming Lin, Natalia Gimelshein, Luca Antiga, et al. Pytorch: An imperative style, high-performance deep learning library. *Advances in neural information processing systems*, 32, 2019.
- [60] John Venables. *Introduction to surface and thin film processes*. Cambridge university press, 2000.